

Local Ionosphere Model Estimation From Dual-Frequency GNSS Observables

by Ryan Mitch and Mark Psiaki
Cornell University, Ithaca, New York

BIOGRAPHY

Ryan Mitch is a Ph.D. student in the Sibley School of Mechanical and Aerospace Engineering at Cornell University. His current research interests are in the areas of GPS systems and model-based estimation. He received his B.S. in Mechanical Engineering from the University of Pittsburgh in 2009.

Mark L. Psiaki is a Professor in the Sibley School of Mechanical and Aerospace Engineering. He received a B.A. in Physics and M.A. and Ph.D. degrees in Mechanical and Aerospace Engineering from Princeton University. His research interests are in the areas of estimation and filtering, spacecraft attitude and orbit determination, and GNSS technology and applications.

ABSTRACT

A method for the removal of ionospheric effects from single-frequency non-GPS radio navigation data through the use of data collected from a single collocated dual-frequency GPS receiver is presented. The method uses a local ionosphere model to estimate the total electron content (TEC) along any line of sight that differs from the GPS satellite lines of sight. Two novel models are investigated, a thick-shell model and a thin-shell model. It is shown that the thin-shell model is more observable than the thick-shell model, and different variations of the thin-shell model are analyzed for utility in this application. A novel method for determining the Gauss-Markov dynamics model tuning parameters using the International Reference Ionosphere (IRI) model is also presented. The algorithm is tested using real GPS observables, and modest improvement is shown over an existing method.

1 INTRODUCTION

A method for the removal of ionospheric effects from single-frequency non-GPS radio navigation data is desired. The strategy adopted uses data from a single collocated dual-frequency GPS receiver. This data is used in conjunction with a local ionosphere model to estimate different lines of sight in the ionosphere, as opposed to kriging, where one attempts to interpolate a random field.

The concept is illustrated in Fig. 1, where \underline{r}_{Rx} is the receiver location and TEC_{L_1, L_2} is the TEC along the GPS satellite lines of sight. The TEC can be measured along the lines of sight to the GPS satellites because they operate on two frequencies. The TEC cannot be measured along the line of sight to the LEO satellite because it only operates on a single-frequency. The additional ionospheric electron content will be approximately removed using the IRI model.

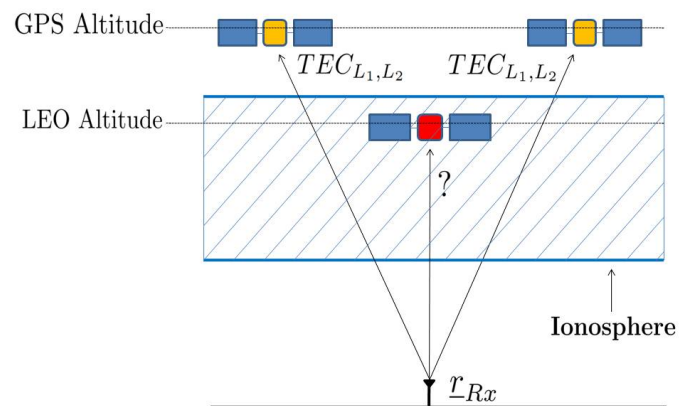


Figure 1 Dual-frequency measurements of the ionosphere used to estimate TEC along other lines of sight

There have been a number of papers that have explored the concept of a local ionosphere model using dual-frequency

receivers. Reference [1] at the University of Calgary used a thin-shell ionosphere model at a fixed altitude, with first and second-order derivatives in Vertical Total Electron Content (VTEC) with respect to latitude and longitude. Reference [2] used a single receiver and created a ‘‘circus tent’’ local ionosphere model, which is effectively a model based on different sections of sight in the elevation and azimuth space. The International GNSS Service [3] also creates global maps of VTEC using a fixed altitude thin-shell model and an array of receivers.

This paper puts forth, and investigates the validity of, two different local ionosphere models. The first is a thick-shell Chapman layer model with latitude and longitude variations in VTEC, scale height, and height of maximum electron density. The second is a thin-shell model with latitude and longitude variations in height and VTEC. Also presented is a new method of using the IRI model to determine an initial starting point for tuning of the filter dynamics model parameters.

This paper starts with the derivation of the relevant GPS observables equations and then moves on to the derivation of the thick-shell and thin-shell local ionosphere models. From there the paper develops a first-order Gauss-Markov dynamics model for use in Extended Kalman Filtering. The parameters of the Gauss-Markov model are derived from batch estimation of the local models using synthesized TEC measurements from the IRI model at the desired receiver location, at intervals throughout a given day. The validity of the local ionosphere models are first evaluated with truth model simulations, and then with batch estimation of TEC measurements constructed from the IRI model. The paper concludes with testing of the presented algorithm using observables from a dual-frequency GPS receiver.

2 IONOSPHERIC IMPACT ON GPS OBSERVABLES

To most GNSS users, the ionospheric effects are typically regarded as a nuisance parameter that degrades the fidelity of the navigation solution. The ways in which the ionosphere affects the GPS observables, through group delay and phase advance, have been described by many authors and will be presented here only briefly, [4], [5] and [6].

The ionosphere acts on the pseudorange or phase of the signal by delaying or advancing it in proportion to the square of its frequency, as shown in Eq. 1.

$$\delta_{Iono}^{sat,j} = 40.3 \frac{TEC_{Rx}^{sat,j}}{f^2} \quad (1)$$

The ionospheric delay shows up in the pseudorange equations, Eqs. 2 and 3, where $P_{Rx,L_1}^{sat,j}$ is the pseudorange from

satellite j to the receiver at the L_1 frequency, $\rho^{sat,j}$ is the actual physical range, c is the speed of light, δt_{Rx} is the receiver clock bias, $\delta t^{sat,j}$ is the satellite clock bias, $\delta_{trop}^{sat,j}$ is the tropospheric delay, $\delta_{Iono,L_1}^{sat,j}$ is the ionospheric delay at the L_1 frequency, $\epsilon_{L_1}^{sat,j}$ is the satellite frequency dependent bias, and ϵ_{Rx,L_1} is the receiver frequency dependent bias. The variables are the same for Eq. 3, but at the L_2 frequency.

$$P_{Rx,L_1}^{sat,j} = \rho^{sat,j} + c(\delta t_{Rx} - \delta t^{sat,j}) + \delta_{trop}^{sat,j} + \delta_{Iono,L_1}^{sat,j} + c(\epsilon_{L_1}^{sat,j} + \epsilon_{Rx,L_1}) \quad (2)$$

$$P_{Rx,L_2}^{sat,j} = \rho^{sat,j} + c(\delta t_{Rx} - \delta t^{sat,j}) + \delta_{trop}^{sat,j} + \delta_{Iono,L_2}^{sat,j} + c(\epsilon_{L_2}^{sat,j} + \epsilon_{Rx,L_2}) \quad (3)$$

The ionospheric delay shows up in the phase equations, as shown in Eqs. 4 and 5, where the repeated variables are the same as in the pseudorange equations, Eqs. 2 and 3. $L_{Rx,L_1}^{sat,j}$ is the phase range from satellite j to the receiver at the L_1 frequency, λ_{L_1} and λ_{L_2} are the wave lengths at L_1 and L_2 frequencies, respectively. $\lambda_{L_1} \Phi_{L_1}^{amb,j}$ and $\lambda_{L_2} \Phi_{L_2}^{amb,j}$ are the phase ambiguities for satellite j at the L_1 and L_2 frequencies, respectively. The variables are the same for Eq. 5, but at the L_2 frequency.

$$L_{Rx,L_1}^{sat,j} = \lambda_{L_1} \Phi_{Rx}^{sat,j} = \rho^{sat,j} + c(\delta t_{Rx} - \delta t^{sat,j}) + \delta_{trop,L_1}^{sat,j} - \delta_{Iono,L_1}^{sat,j} + c(\epsilon_{L_1}^{sat,j} + \epsilon_{Rx,L_1}) + \lambda_{L_1} \Phi_{L_1}^{amb,j} \quad (4)$$

$$L_{Rx,L_2}^{sat,j} = \lambda_{L_2} \Phi_{Rx}^{sat,j} = \rho^{sat,j} + c(\delta t_{Rx} - \delta t^{sat,j}) + \delta_{trop,L_2}^{sat,j} - \delta_{Iono,L_2}^{sat,j} + c(\epsilon_{L_2}^{sat,j} + \epsilon_{Rx,L_2}) + \lambda_{L_2} \Phi_{L_2}^{amb,j} \quad (5)$$

The paper develops its Kalman Filter measurement model by taking the single difference of both the pseudorange and phase equations, to produce Eqs. 6 and 7, where $\Delta P_{Rx}^{sat,j}$ is the difference in the pseudoranges on the L_1 and L_2 frequencies, $\Delta T_{CB}^{sat,j}$ is satellite j 's interfrequency pseudorange delay (code bias), and $\Delta T_{CB,Rx}$ is the receiver interfrequency pseudorange delay. In addition, $\Delta \rho^{amb,j}$ is the difference in the phase ambiguities at the L_1 and L_2 frequencies. The single difference removes the actual range between the receiver and satellite along a given line of sight (LOS), the satellite clock bias, the receiver clock bias and the tropospheric delay.

$$\Delta P_{Rx}^{sat,j} = P_{Rx,L_2}^{sat,j} - P_{Rx,L_1}^{sat,j} = (\delta_{Iono,L_2}^{sat,j} - \delta_{Iono,L_1}^{sat,j}) - c(\Delta T_{CB}^{sat,j}) - c(\Delta T_{CB,Rx}) \quad (6)$$

LOCAL THICK-SHELL MODEL WITH ALTI- TUDE AND THICKNESS VARIATIONS

$$\begin{aligned} \Delta L_{Rx}^{sat,j} &= L_{Rx,L_1}^{sat,j} - L_{Rx,L_2}^{sat,j} = (\delta_{Iono,L_2}^{sat,j} - \delta_{Iono,L_1}^{sat,j}) \\ &\quad + c(\Delta T_{CB}^{sat,j}) + c(\Delta T_{CB,Rx}) + \Delta \rho^{amb,j} \end{aligned} \quad (7)$$

$$\Delta \rho^{amb,j} = \lambda_{L_1} \Phi_{L_1}^{amb,j} - \lambda_{L_2} \Phi_{L_2}^{amb,j} \quad (8)$$

The differenced pseudorange equations provide an unambiguous, but noisy, measurement of TEC. The phase measurements are much more precise, with about an order of magnitude less noise, but they require estimation of the delta phase ambiguities, Eq. 8. The receiver code bias and satellite biases drift very slowly and will be assumed to stay constant over a full day. Reference [7] showed that the day-to-day variations of the satellite interfrequency code biases over a five week span are less than 0.3 ns, and receiver biases are on the order of 0.5 ns. The satellite code bias is provided by JPL, with approximately one week latency, and will be assumed to be compensated for in the rest of this paper.

This assumption is necessary because a single dual-frequency receiver cannot estimate the satellite biases. The use of old satellite biases will introduce some errors in the final filter results, but they should have an acceptably small magnitude.

Rearranging Eqs. 6 and 7, and using the first-order model approximation of range delay and phase advance, Eq. 1, one arrives at the final measurement model equations, Eqs. 9 and 10, where f_{L_1} is the L_1 frequency and f_{L_2} is the L_2 frequency. One should take note that the TEC terms have the same sign and the interfrequency bias terms have the opposite sign because of an intentional sign reversal between the definitions of the pseudorange and phase single differences in Eqs. 6 and 7.

$$\begin{aligned} \Delta P_{Rx}^{sat,j} &= 40.3 \left(\frac{f_{L_1}^2 - f_{L_2}^2}{f_{L_1}^2 f_{L_2}^2} \right) TEC_{Rx}^{sat,j} \\ &\quad - c(\Delta T_{CB}^{sat,j} + \Delta T_{CB,Rx}) \end{aligned} \quad (9)$$

$$\begin{aligned} \Delta L_{Rx}^{sat,j} &= 40.3 \left(\frac{f_{L_1}^2 - f_{L_2}^2}{f_{L_1}^2 f_{L_2}^2} \right) TEC_{Rx}^{sat,j} \\ &\quad + c(\Delta T_{CB}^{sat,j} + \Delta T_{CB,Rx}) + \Delta \rho^{amb,j} \end{aligned} \quad (10)$$

TEC is defined as the integrated electron density between the receiver and satellite.

$$TEC = \int_{Rx}^{sat} \rho_{elec}(LOS, \alpha) d\alpha \quad (11)$$

The GPS satellites provide an estimate of TEC along GPS satellite lines of sight, but give no information about TEC along other lines of sight. Local ionosphere models can provide the means to predict TEC along other lines of sight. Two local ionosphere models are presented, a thick-shell model and a thin-shell model. The thick-shell model is derived from the Chapman profile [8], which is a simple profile that is used to describe the variation of electron density with altitude.

The Chapman profile in Fig. 2 is created using Eq. 12, where h_{scale} is related to the width of the profile, h_{max} is the altitude of maximum electron density, and ρ_{max} is the maximum electron density. This profile can also be formulated using VTEC instead of ρ_{max} , as shown in Eq. 13.

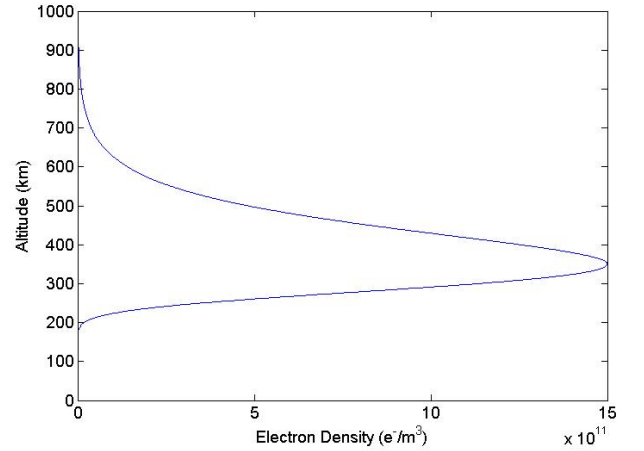


Figure 2 An example Chapman profile, with the parameters $h_{max} = 350$ km, $h_{scale} = 75$ km, and $\rho_{max} = 1.5 * 10^{12}$ elec/m³

$$\rho_{elec} = \rho_{max} e^{[1 - z_{chap} - e^{-z_{chap}}]} \quad (12)$$

$$\rho_{elec} = \left[\frac{VTEC}{e^1 h_{scale}} \right] e^{[1 - z_{chap} - e^{-z_{chap}}]} \quad (13)$$

Where,

$$z_{chap} = \frac{h - h_{max}}{h_{scale}} \quad (14)$$

is a non-dimensional altitude, and h is the height that the profile is evaluated at.

The electron density profile of Eq. 13 can be modified to allow variations in VTEC, h_{scale} and h_{max} with respect to latitude and longitude. The Chapman profile is centered on the location of maximum electron density, h_{max} . It is important to realize that in this local model the Chapman

profile is defined *not* along the local vertical, but along the local normal to the h_{max} surface, as shown in Fig 3. The electron density of any point off of the h_{max} surface is evaluated by finding the nearest point on the h_{max} surface, and then evaluating the Chapman profile associated with that point.

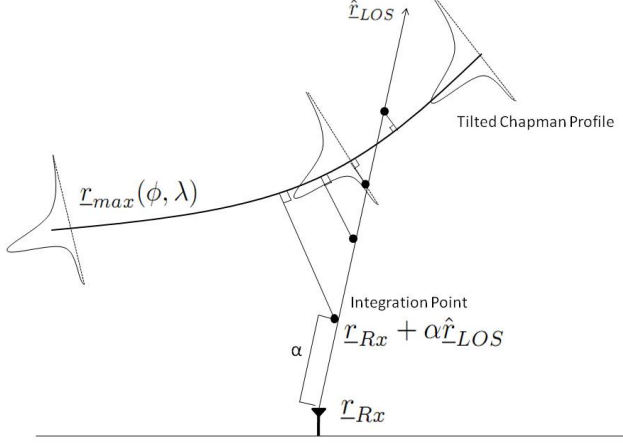


Figure 3 Geometry of the thick-shell density model and TEC calculation

In Fig. 3, the curve above the receiver, $r_{max}(\phi, \lambda)$, is the line of maximum electron density, the arrow, \hat{r}_{LOS} , is the line of sight and the dots are the integration points. α is the distance along the line of sight, from the receiver to the satellite, at which one wishes to evaluate the model.

The thick-shell model is parameterized by three second-order Taylor Series Expansions, one for its height of maximum electron density, one for its scale height, and one for its VTEC. Each Taylor Series is a two-dimensional function of latitude and longitude perturbation from the receiver location. These perturbations are measured at the points on the h_{max} surface.

$$h_{max} = h_{max_0} + \frac{dh_{max}}{d\phi} \Delta\phi_n + \frac{dh_{max}}{d\lambda} \Delta\lambda_n + \frac{1}{2} \frac{d^2 h_{max}}{d^2 \phi} \Delta\phi_n^2 + \frac{d^2 h_{max}}{d\phi d\lambda} \Delta\phi_n \Delta\lambda_n + \frac{1}{2} \frac{d^2 h_{max}}{d^2 \lambda} \Delta\lambda_n^2 \quad (15)$$

$$h_{scale} = h_{scale_0} + \frac{dh_{scale}}{d\phi} \Delta\phi_n + \frac{dh_{scale}}{d\lambda} \Delta\lambda_n + \frac{1}{2} \frac{d^2 h_{scale}}{d^2 \phi} \Delta\phi_n^2 + \frac{d^2 h_{scale}}{d\phi d\lambda} \Delta\phi_n \Delta\lambda_n + \frac{1}{2} \frac{d^2 h_{scale}}{d^2 \lambda} \Delta\lambda_n^2 \quad (16)$$

$$VTEC = VTEC_0 + \frac{dVTEC}{d\phi} \Delta\phi_n + \frac{dVTEC}{d\lambda} \Delta\lambda_n + \frac{1}{2} \frac{d^2 VTEC}{d^2 \phi} \Delta\phi_n^2 + \frac{d^2 VTEC}{d\phi d\lambda} \Delta\phi_n \Delta\lambda_n + \frac{1}{2} \frac{d^2 VTEC}{d^2 \lambda} \Delta\lambda_n^2 \quad (17)$$

The process of determining the electron density at an arbitrary point is complicated. Suppose one wants to determine electron density at the following point along the line of sight direction unit vector:

$$r_{Rx} + \alpha \hat{r}_{LOS} \quad (18)$$

where r_{Rx} is the receiver location. Suppose this density is called $\rho_{LOS}(\alpha)$. The calculation starts by determining the nearest point on the h_{max} surface:

$$r_n(\alpha) = r_{max}[\phi_n(r_{Rx} + \alpha \hat{r}_{LOS}), \lambda_n(r_{Rx} + \alpha \hat{r}_{LOS})] \quad (19)$$

where n stands for “nearest”, and $\phi_n(r_{Rx} + \alpha \hat{r}_{LOS})$ and $\lambda_n(r_{Rx} + \alpha \hat{r}_{LOS})$ are the latitude and longitude of the nearest point on the h_{max} surface. The functions $\phi_n(r_{Rx} + \alpha \hat{r}_{LOS})$ and $\lambda_n(r_{Rx} + \alpha \hat{r}_{LOS})$ must be evaluated via numerical optimization. This optimization uses the definitions:

$$\Delta\phi_n = \phi_n(r_{Rx} + \alpha \hat{r}_{LOS}) - \phi_{Rx} \quad (20)$$

$$\Delta\lambda_n = \lambda_n(r_{Rx} + \alpha \hat{r}_{LOS}) - \lambda_{Rx} \quad (21)$$

and the function $r_{max}(\phi_n, \lambda_n)$, which can be defined based on Eq. 15 and the WGS 84 ellipsoid. The optimization seeks the ϕ_n and λ_n that minimize $\|r_{max}(\phi_n, \lambda_n) - r_{Rx} - \alpha \hat{r}_{LOS}\|$. This minimization results in the perpendicularity condition that is demonstrated in Fig. 3.

Given $r_n(\alpha)$ and the associated $\Delta\phi_n$ and $\Delta\lambda_n$, one can evaluate Eqs. 16 and 17 to determine h_{scale} and VTEC. One can then use $r_n(\alpha)$ and h_{scale} to compute:

$$z_{chap} = \frac{\|r_{Rx} + \alpha \hat{r}_{LOS} - r_n\|}{h_{scale}} \quad (22)$$

and one can use these results in Eq. 13 to compute $\rho_{LOS}(\alpha)$.

Determining the TEC from the calculation of individual $\rho_{LOS}(\alpha)$ s requires numerical integration:

$$TEC = \int_{Rx}^{sat} \rho_{LOS(\alpha)} d\alpha \approx \sum_{i=1}^N \rho_{LOS(\alpha)} \Delta\alpha \quad (23)$$

Integration will require evaluation of the local model at numerous points along any given line of sight. Quadrature integration using 125 points along the line of sight, spaced evenly between z_{chap} of -4 and 30, results in an accuracy of 1 part in 10^{10} .

The benefits of this local model versus that of the next model, the thin-shell model, is that it is based on an electron distribution profile. If this local model can be accurately fit to the local ionosphere, then numerical integration of this model will be more accurate than the thin-shell model.

The downsides of this model are that many of the states are weakly observable, namely h_{scale} and h_{max} , and there is an increase in computation time over the thin-shell model. The reason for the weak observability is that one receives data in the form of TEC, which does not contain much information about the distribution *within* the profile. This local ionosphere model can use up to 18 parameters, the 18 Taylor Series coefficients in Eqs 15 - 17. These coefficients can be difficult to estimate when the maximum number of GPS satellites observable at any given time is 12, even with a time series of measurements. This model can be truncated as necessary by constraining certain Taylor Series coefficients. The usefulness of this model is investigated further in section 4.

LOCAL THIN-SHELL MODEL WITH ALTITUDE VARIATIONS

In the local thin-shell ionosphere, the thickness is assumed to be compressed into an infinitesimal layer at a given altitude, with h_{scale} effectively set to zero, as shown in Fig. 4.

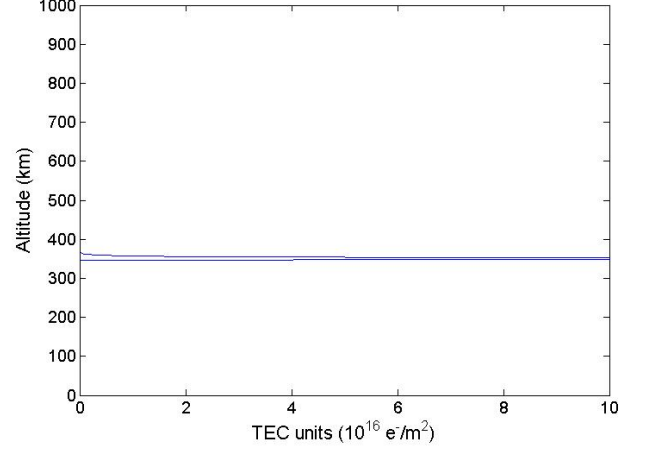


Figure 4 The electron density profile of the thin-shell model can be thought of as an impulse function in TEC at a given altitude

The local thin-shell ionosphere model is similar to the thick-shell model in that it allows variations of VTEC and altitude with respect to latitude and longitude, as shown in Fig. 5.

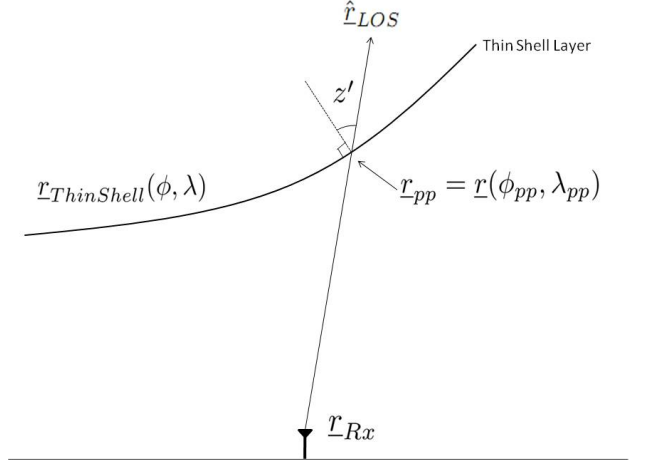


Figure 5 Geometry of the local ionosphere thin-shell layer and of TEC evaluation at the pierce point

The TEC along any given line of sight is equal to the VTEC (actually the TEC perpendicular to the thin-shell layer) at the pierce point multiplied by a mapping function. The mapping function used in this paper is equal to one divided by the cosine of the angle made by the line of sight and the normal of the shell at the pierce point, as shown in Eq. 24.

$$TEC = VTEC \frac{1}{\cos(z')} \quad (24)$$

There are many other forms of the mapping function [9] but they are not considered in this paper.

The height and VTEC states are allowed to vary with respect to latitude and longitude using a second-order Taylor Series Expansion.

$$h = h_0 + \frac{dh}{d\phi} \Delta\phi_{pp} + \frac{dh}{d\lambda} \Delta\lambda_{pp} + \frac{1}{2} \frac{d^2h}{d^2\phi} \Delta\phi_{pp}^2 + \frac{d^2h}{d\phi d\lambda} \Delta\phi_{pp} \Delta\lambda_{pp} + \frac{1}{2} \frac{d^2h}{d^2\lambda} \Delta\lambda_{pp}^2 \quad (25)$$

$$VTEC = VTEC_0 + \frac{dVTEC}{d\phi} \Delta\phi_{pp} + \frac{dVTEC}{d\lambda} \Delta\lambda_{pp} + \frac{1}{2} \frac{d^2VTEC}{d^2\phi} \Delta\phi_{pp}^2 + \frac{d^2VTEC}{d\phi d\lambda} \Delta\phi_{pp} \Delta\lambda_{pp} + \frac{1}{2} \frac{d^2VTEC}{d^2\lambda} \Delta\lambda_{pp}^2 \quad (26)$$

The thin-shell ionosphere model does not require integration because the electron density is all concentrated at one altitude, and $\Delta\phi_{pp}$ and $\Delta\lambda_{pp}$ are evaluated at the single pierce point:

$$\Delta\phi_{pp} = \phi_{pp} - \phi_{Rx} \quad (27)$$

$$\Delta\lambda_{pp} = \lambda_{pp} - \lambda_{Rx} \quad (28)$$

3 EXTENDED SQUARE ROOT INFORMATION FILTERING OF MEASUREMENT TIME HISTORIES

Kalman Filtering is typically used when there is some form of correlation between model states from one time epoch to the next, and when one wants an optimal state estimate. The Extended Square Root Information Filter is one form of the Extended Kalman Filter that linearizes about the current state estimate, has favorable numerical stability properties, and is computationally efficient. The state temporal correlation is formulated using a dynamics model.

FILTER DYNAMICS MODEL

The dynamics model for this system does not use any physical dynamics of the ionosphere for a number of reasons,

specifically because of the level of complexity that would be required and because of observability issues. Instead, this model attempts to capture the temporal correlation between states through the use of a first-order Gauss-Markov process on the perturbation of the state from a nominal state value. This model takes the following form:

$$\dot{\underline{x}}_{Iono} = \begin{bmatrix} \frac{-1}{\tau_{Iono,1}} & 0 & \dots & 0 \\ 0 & \frac{-1}{\tau_{Iono,2}} & \ddots & \vdots \\ \vdots & \ddots & \ddots & 0 \\ 0 & \dots & 0 & \frac{-1}{\tau_{Iono,n}} \end{bmatrix} (\underline{x}_{Iono} - \underline{x}_{IonoRef}) + \begin{bmatrix} \sigma_{Iono,1} \sqrt{\frac{2}{\tau_{Iono,1}}} & 0 & \dots & 0 \\ 0 & \sigma_{Iono,2} \sqrt{\frac{2}{\tau_{Iono,2}}} & \ddots & \vdots \\ \vdots & \ddots & \ddots & 0 \\ 0 & \dots & 0 & \sigma_{Iono,n} \sqrt{\frac{2}{\tau_{Iono,n}}} \end{bmatrix} \underline{w} \quad (29)$$

where \underline{x}_{Iono} is the ionospheric state vector, the τ_{Iono} s are the state correlation time constants, \underline{w} is the zero-mean unit-power-spectral-density process noise input vector, and σ_{Iono} s are the steady state standard deviations of the elements of \underline{x}_{Iono} from their nominal values, which are contained in $\underline{x}_{IonoRef}$.

The reference vector, $\underline{x}_{IonoRef}$, is used because one can reasonably assume that the ionosphere will remain relatively near a nominal value. This reference state can be considered a tuning parameter, where the following reference values were used: 350 km for h_{max} , 50 km for h_{scale} and 10 TECU for VTEC during the day. This reference state could be modified to a daily time varying reference if enough data were available to form a reasonable guess.

Note:

$$\underline{x}_{Iono} = \begin{bmatrix} \underline{x}_h \\ \underline{x}_{VTEC} \end{bmatrix}, \text{ or } \begin{bmatrix} \underline{x}_{h_{max}} \\ \underline{x}_{h_{scale}} \\ \underline{x}_{VTEC} \end{bmatrix} \quad (30)$$

where the left hand expression is used for the thin-shell ionosphere model, and the right hand expression is used for the thick-shell ionosphere model. The vector \underline{x}_h consists of the unknown Taylor series coefficients in Eq. 25, the vector $\underline{x}_{h_{max}}$ consists of the unknown coefficients in Eq. 15. The vector $\underline{x}_{h_{scale}}$ contains the Taylor Series coefficients of Eq. 16. The vector \underline{x}_{VTEC} contains the unknown coefficients from Eq. 17 or 26, depending on whether the thin-shell or thick-shell model is being used.

Determining τ and σ can be difficult, as these parameters could vary greatly from location to location and from

day to day. In an attempt to quantify the best-case, low-ionospheric-activity values of the dynamics model tuning parameters, the IRI model was used in a non-linear batch estimation scheme.

The IRI model, Reference [10], provides a basic distribution of electrons around the earth. This model can be evaluated at a number of points along a given line of sight and then combined with an integration scheme to obtain the TEC along a given line of sight. Once a receiver location is identified, the TEC along many lines of sight can be determined throughout the course of a full day. These TEC values can be considered as TEC “measurements” from a calibrated dual-frequency receiver. One can then use a Gauss-Newton batch estimator to fit the thin-shell or thick-shell local ionosphere models to the measurements at a single time epoch. This process can be repeated sequentially throughout the day.

The τ and σ values of each state can be backed out of this process by looking at the normalized correlation of each state throughout the day. Fig. 6 is a plot of the batch estimates of the $VTEC_0$ state (VTEC directly above the receiver) throughout the course of a day. Fig. 7 is the normalized correlation plot. The time constant τ will equal the time for the normalized correlation value to go below e^{-1} , and σ will be initially based on the standard deviation of the state over the day. The corresponding value of $\underline{x}_{IonoRef}$ could be taken as the mean throughout the day, although this was not always the case in the present study.

It is important to fit only the number of states of the local ionosphere model that one will actually use when filtering, because the resulting τ and σ parameters can vary for different state combinations (i.e. Taylor series coefficient combinations).

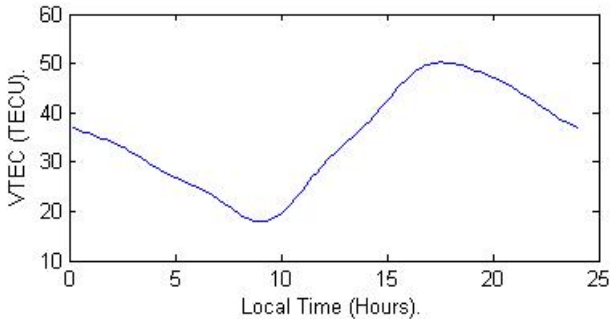


Figure 6 The batch estimate of VTEC above the receiver throughout the day

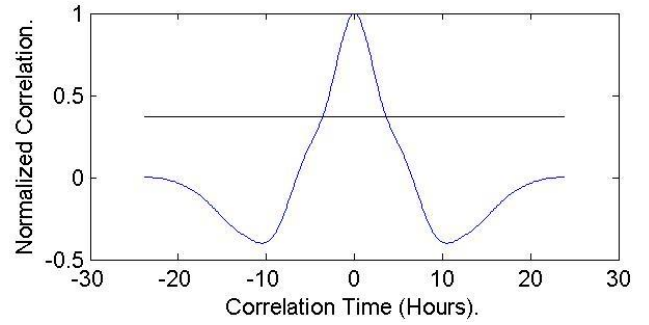


Figure 7 The normalized correlation plot of the VTEC state over the day

The above method of determining the dynamics model tuning parameters is not robust. Therefore, in actual implementation the dynamics model tuning parameters τ and σ will be different. The correlation and noise will likely both be scaled down by the same factor. The parameters determined from the IRI model provide a starting point for tuning of the final dynamics model parameters. The results of this batch estimation scheme for a given day, and for three different models, are listed in Tables 1 and 2 in section 4.

Some practitioners in this field pick τ and σ values based on experience, [2] and [1], but the present authors preferred the method defined above because of a lack of experience. The above practitioners likely performed additional tuning once they had experience using real data.

FILTER MEASUREMENT MODEL

The measurement model for this system is effectively a nesting of the local ionosphere measurement model inside a GPS single difference observables measurement model:

$$\underline{y} = \begin{bmatrix} \underline{h}_P(\underline{x}) \\ \underline{h}_L(\underline{x}) \end{bmatrix} + \underline{\nu} = \begin{bmatrix} \Delta P^1 \\ \vdots \\ \Delta P^j \\ \Delta L^1 \\ \vdots \\ \Delta L^j \end{bmatrix} + \underline{\nu} \quad (31)$$

where the measurement function $\underline{h}_P(\underline{x})$ is defined by the single difference pseudorange equation, Eq 9; and $\underline{h}_L(\underline{x})$ is defined by the single phase difference equation, Eq 10.

The full state of this system, \underline{x} , includes the ionospheric state vector, but it has been augmented to include the nuisance parameters of receiver code bias and delta phase ambiguities:

$$\underline{x} = \begin{bmatrix} \Delta T_{CB,Rx} \\ \Delta \rho^{amb,j} \\ \underline{x}_{Iono} \end{bmatrix} = \begin{bmatrix} \Delta T_{CB,Rx} \\ \Delta \rho^{amb,1} \\ \vdots \\ \Delta \rho^{amb,j} \\ \underline{x}_{Iono} \end{bmatrix} \quad (32)$$

Extended Kalman Filters require the measurement sensitivity matrix, the Jacobians $\frac{\partial h_P}{\partial \underline{x}}$ and $\frac{\partial h_L}{\partial \underline{x}}$, in order to determine the optimal state estimate. It takes the form of the top part of Eq. 33, where the second line simplifies the nuisance parameters.

$$\begin{aligned} H = \frac{\partial h}{\partial \underline{x}} &= \begin{bmatrix} \frac{\partial h_P}{\partial \Delta T_{CB,Rx}}, \frac{\partial h_P}{\partial \Delta \rho^{amb,j}}, \frac{\partial h_P}{\partial \underline{x}_{Iono}} \\ \frac{\partial h_L}{\partial \Delta T_{CB,Rx}}, \frac{\partial h_L}{\partial \Delta \rho^{amb,j}}, \frac{\partial h_L}{\partial \underline{x}_{Iono}} \end{bmatrix} \\ &= \begin{bmatrix} -c * \underline{e}, \underline{I}, \frac{\partial h_P}{\partial \underline{x}_{Iono}} \\ -c * \underline{e}, \underline{0}, \frac{\partial h_L}{\partial \underline{x}_{Iono}} \end{bmatrix} \end{aligned} \quad (33)$$

Where:

$$\underline{e} = \begin{bmatrix} 1 \\ \vdots \\ 1 \end{bmatrix} \quad (34)$$

FILTER MECHANICS

This project used an Extended Square Root Information Filter (ESRIF), which is a more numerically stable form of the Extended Kalman Filter. The reader is assumed to have some familiarity with this type of filter, and its formulation is not presented here. Reference [11] contains further information on Extended Kalman Filters, and reference [12] contains further information on Square Root Information Filters.

The uncertainties of TEC along a given line of sight can be understood through a plot of a surface composed of TEC uncertainty along many lines of sight versus their azimuths and elevations. The uncertainties are calculated as follows:

$$\underline{P}_{TEC,LOS} = \sqrt{\left(\frac{\partial TEC_{LOS}}{\partial \underline{x}_{Iono}} \right) P_{xx,Iono} \left(\frac{\partial TEC_{LOS}}{\partial \underline{x}_{Iono}} \right)^T} \quad (35)$$

where $P_{xx,Iono}$ is the Kalman Filter state estimation error covariance matrix for the ionospheric states, and $\frac{\partial TEC_{LOS}}{\partial \underline{x}_{Iono}}$

is the local ionosphere model measurement sensitivity matrix, similar to Eq. 33. This equation is a linearized approximation of how uncertainty propagates through the ionosphere model. An example contour has been plotted in Fig. 8.

The plot has been generated using a thin-shell model with a single altitude at 350km and with full VTEC derivatives. The uncertainties result from a specific two hour span of GPS observables. The uncertainties in derivatives with respect to latitude and longitude cause the azimuthal ripples in the surface.

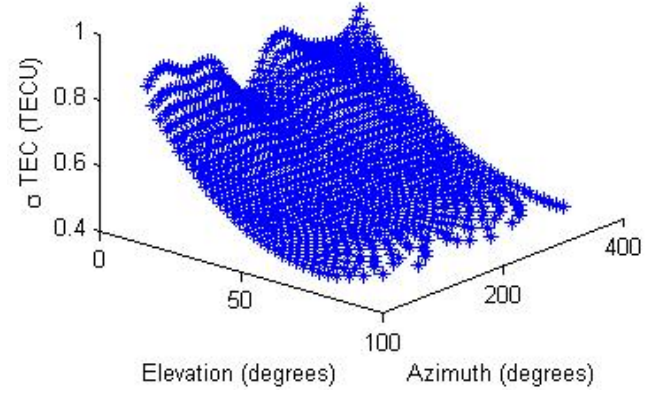


Figure 8 A surface of 1- σ TEC uncertainties versus line-of-sight azimuths and elevations

4 RESULTS

LOCAL IONOSPHERE MODEL EVALUATIONS

The benefits and limitations of both the thick-shell and thin-shell ionosphere models will be investigated in order to determine the better model for the desired application. The ideal model would emulate the true physics of the ionosphere so that the model could accurately predict the TEC along lines of sight not in its measurement set, but with a small enough number of states to preserve observability.

Intuitively, one would think that the thick-shell ionosphere model would be the best model to use because it captures the distribution of electron density with respect to altitude and provides a larger number of variable states. With an unlimited number of TEC measurements, the thick-shell model would be superior. The benefits of the thick-shell model however, are offset by the weak observability of the extra states and by a considerable increase in computation time.

These models will be evaluated with two criteria,

observability-state tracking and ionospheric emulation fidelity.

CRITERION 1: OBSERVABILITY-STATE TRACKING (TRUTH MODEL SIMULATION)

A truth model simulation, using measurements created from exactly the same measurement model as that used by the Kalman Filter, can test a necessary condition for observability. The logic of this test is the following: if a Kalman Filter cannot track its own model, given a long data run and pure Gaussian white noise, then it will not be able to emulate and track the true ionosphere.

The following truth model simulation was initialized with a state vector of h_{max} equal to 350 km, h_{scale} equal to 50 km, VTEC equal to 20 TECU, and time constants of 100 minutes. The Markov process steady state standard deviations were set to 40 km on h_{max} , 25 km on h_{scale} and 10 TECU, on VTEC and their derivatives. The simulation used 7 satellites and two hours worth of data, with measurement noise standard deviations of 0.1 TECU, consistent with carrier phase-based TEC measurements. The same set of GPS satellite position time histories have been used throughout this paper, and they represents a real configuration of the GPS constellation. Future studies will use additional satellite geometries.

Figs. 9, 10 and 11 contain plots of the truth (thick black line), estimate (red line) and 1-sigma error bounds on the state estimates (blue lines) of all 18 states, h_{max} , h_{scale} and VTEC. The results are a good indicator of the relative observability of the ionosphere model's states. It becomes clear that h_{scale} and its derivatives are weakly observable, as are the second derivatives of h_{max} .

The steady state standard deviations on the second derivatives of h_{max} and h_{scale} are equal to or *greater* than the standard deviations given to the dynamics model. This result means that the time history of the TEC measurements was not able to improve the certainty of those states beyond what was originally provided to the dynamics model, despite the long temporal correlation. It seems that h_{max} and its first derivatives are observable, but that h_{scale} is weakly observable, if at all. The VTEC states are all observable, with standard deviations reduced from the values provided to the dynamics model.

The above analysis was repeated for the thick-shell with the second derivatives in height removed, and then with first derivatives removed. The results were very similar to the previous simulation, but with slightly higher observability on the remaining height states due to the reduction in the total number of states. The h_{scale} derivatives were still unobservable, but the nominal value directly above the receiver was slightly observable.

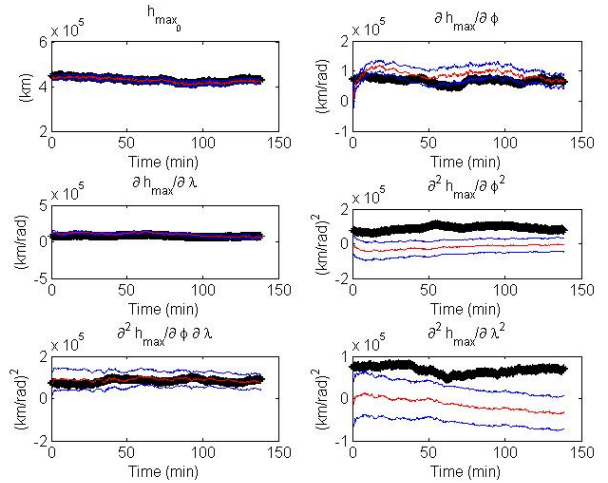


Figure 9 h_{max} and its derivatives with respect to latitude (ϕ) and longitude (λ)

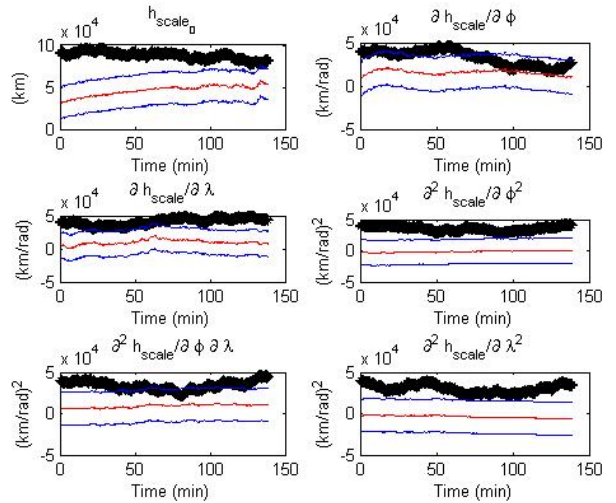


Figure 10 h_{scale} and its derivatives with respect to latitude (ϕ) and longitude (λ)

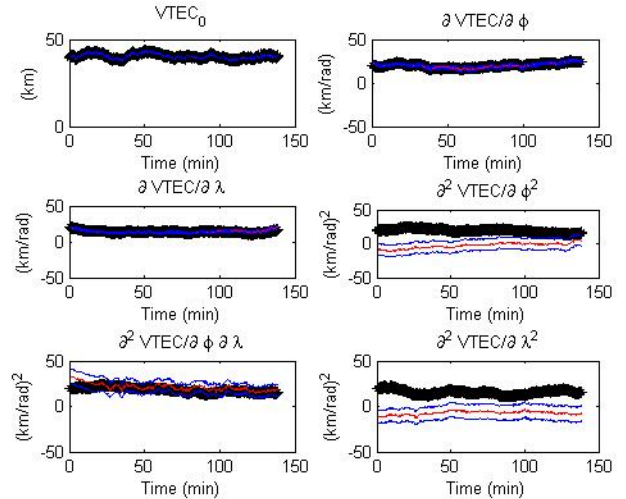


Figure 11 VTEC and its derivatives with respect to latitude (ϕ) and longitude (λ)

A recommended implementation based on state observability would contain the nominal over-head value of h_{max} , its latitude and longitude first derivatives, h_{scale} , VTEC and all of VTEC's latitude and longitude derivatives. The low observability states make the thick-shell local ionosphere model difficult to use, and as a result, it will not be considered further in this paper.

Similar to the thick-shell model, the capabilities and limitations of the thin-shell model have been tested with a thin-shell truth model simulation, but with plots not included. The thin-shell truth model simulation used the same parameters and initial state values as the thick-shell model, but with the h_{scale} terms removed.

The thin-shell truth model simulation result is that the VTEC states are strongly observable and that the heights are moderately observable, with the second derivatives on height being only weakly observable. Any combination of Taylor Series coefficient states on the local thin-shell ionosphere model will work, and these combinations are investigated further using the second criterion.

CRITERION 2: EMULATION FIDELITY FOR THE IRI MODEL

This section investigates the abilities of various local thin-shell ionosphere models to represent the behavior of the true ionosphere. The investigation involves batch estimation of the model states in an attempt to fit the IRI model TEC values.

The four different models considered are depicted graphically in Fig. 12. Model 1 is a fixed altitude (350 km) model with full derivatives with respect to latitude and longitude of VTEC. Model 2 is the same as Model 1, but with a varying altitude that must be estimated. Models 3 and 4 are the same as Model 2, but with first and second-order derivatives on height. Model 3 only considers first derivatives, and Model 4 considers both first and second derivatives. The graphic in Fig. 12 illustrates these differences by showing the different models' possibilities for their thin height contours.

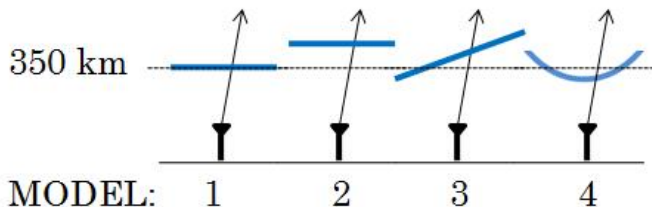


Figure 12 Representative height contours for the 4 thin-shell ionosphere models

The TEC values for the IRI model have been computed along 100 lines of sight spaced evenly about elevation and

azimuth with an elevation mask of 15 degrees. The above evaluation is done for a single location and for 3 times spaced evenly throughout the day. The density along each line of sight has been evaluated at 300 points spaced evenly from the theoretical receiver to the theoretical satellite, as high as the IRI model would allow (60-2000km), and the points were integrated to evaluate the TEC along each line of sight, with an expected TEC error of less than 0.001 TECU.

A subset of the TEC measurements was randomly selected and used to batch estimate the local ionosphere models, without added measurement noise. The estimated local ionosphere models were then used to calculate the TEC along the full 100 lines of sight. The model TEC predictions along the full 100 lines of sight were compared against the actual computed IRI values, and the RMS TEC error was calculated. Fig. 13 plots the RMS TEC error against the number of measurements used in the local ionosphere estimate for the 4 thin-shell models.

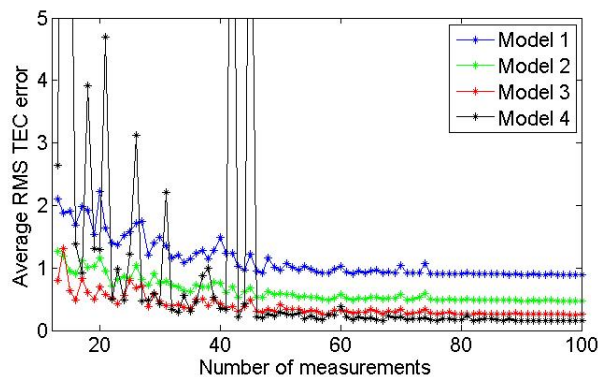


Figure 13 RMS TEC errors of 4 thin-shell ionosphere models over 100 lines of sight, with varying numbers of measurements used to fit the individual batch estimates

The results of the IRI batch estimation support what one might have expected. There are two important regions in the graph, the region with a high number of measurements used explicitly in the batch fit, above 75 measurements, and the region with a low number of measurements, below 45 measurements.

The region with a high number of measurements demonstrates the ability of each model to capture the true behavior of the IRI model. The more states available, the better the model fit to the measurements. The best emulation of the ionosphere comes from Model 4, and Models 3, 2 and 1 have decreasing levels of fidelity. Note however, that even Model 1 can achieve a RMS fit error of less than 1 RMS TECU error, which might be sufficient for many applications.

The region with a low number of measurements demonstrates the relative observability of each model. Low observability issues are the most evident in Model 4, where

there are very large RMS TEC errors, even when there are up to 45 measurements. These large RMS errors imply poor observability. Therefore, Model 4 should not be used unless there are a very high number of measurements, likely more than are available from the GPS constellation. Model 4 will not be considered further in this paper.

The number of measurements available, and their spread in elevation and azimuth, will determine the appropriate model implementation. If there are many satellites that are evenly spaced in the sky, then one might want to use the model with first-order height derivatives. If there are only a few satellites visible, then it may be best to let the altitude have only one single estimated variable, its nominal height above the receiver. The filter will estimate this value along with the VTEC states, or it may simply fix the altitude at a specified value.

The results of IRI batch estimation of the Markov process dynamics model tuning parameters, τ and σ , are listed in Tables 1 and 2. Blanks in the table indicate parameters not used in the given model.

Table 1 The Markov process τ values that have been derived from IRI batch estimation

τ (min) of the Taylor Series Coefficients:	Model 1	Model 2	Model 3
h_0	-	119	218
$\frac{dh}{d\phi}$	-	-	216
$\frac{dh}{d\lambda}$	-	-	134
$\frac{d^2h}{d\phi^2}$	-	-	-
$\frac{d^2h}{d\phi d\lambda}$	-	-	-
$\frac{d^2h}{d\lambda^2}$	-	-	-
VTEC ₀	260	258	258
$\frac{dVTEC}{d\phi}$	248	249	246
$\frac{dVTEC}{d\lambda}$	189	187	192
$\frac{d^2VTEC}{d\phi^2}$	177	279	122
$\frac{d^2VTEC}{d\phi d\lambda}$	216	212	203
$\frac{d^2VTEC}{d\lambda^2}$	189	288	271

Table 2 The Markov process steady state σ values that have been derived from IRI batch estimation

σ of the Taylor Series Coefficients:	Model 1	Model 2	Model 3
h_0 (km)	-	3479	37655
$\frac{dh}{d\phi}$ (km/rad)	-	-	9968
$\frac{dh}{d\lambda}$ (km/rad)	-	-	6479
$\frac{d^2h}{d\phi^2}$ (km/rad) ²	-	-	-
$\frac{d^2h}{d\phi d\lambda}$ (km/rad) ²	-	-	-
$\frac{d^2h}{d\lambda^2}$ (km/rad) ²	-	-	-
VTEC ₀ (TECU)	1.84	1.85	3.38
$\frac{dVTEC}{d\phi}$ (TECU/rad)	3.82	3.29	2.60
$\frac{dVTEC}{d\lambda}$ (TECU/rad)	1.62	1.40	1.19
$\frac{d^2VTEC}{d\phi^2}$ (TECU/rad) ²	8.40	9.95	2.77
$\frac{d^2VTEC}{d\phi d\lambda}$ (TECU/rad) ²	9.17	6.05	4.61
$\frac{d^2VTEC}{d\lambda^2}$ (TECU/rad) ²	8.32	11.96	10.18

FILTER EVALUATION USING REAL GPS DATA

The final validation step used dual-frequency GPS observables from Arecibo, Puerto Rico. Data were recorded for a two hour span during the first day of the year 2010, and the data were trimmed to include only the seven continuously available satellites (continuous phase arcs).

To test the TEC predictive abilities of the proposed algorithm, one satellite was removed from the measurement set, and the state was estimated based on the remaining 6 satellites. The predicted TEC along the removed line of sight was then compared against the actual TEC measurement as determined from the ΔL carrier phase measurement, with compensation of the necessary parameters for that line of sight. The compensation used the delta phase ambiguity, $\Delta\rho^{amb,j}$, as estimated from the 7 satellite set, and the receiver interfrequency bias, $\Delta T_{CB,Rx}$, as estimated from the 6 satellite set. This process has been repeated 7 times, deleting a different satellite from the filter's measurement set for each of the 7 implementations. RMS TEC prediction errors were then computed for each filter model based on its 7 prediction errors.

The filter was tuned based on the measurement set in order to improve the performance. The final values of τ and σ were about one half to one fifth of the values predicted based on batch estimation of the IRI model. This tuning makes intuitive sense because the development of the IRI model used monthly averages of data, and the IRI model is expected to capture only general behavior.

In an attempt to put the results into context, the same algorithm was run using the fixed altitude model of Reference [1]. The time constants used by Reference [1] were 1800 seconds for all states, the σ s were set to 2 (TECU) for receiver VTEC₀, 0.5 (TECU/rad) for $\frac{\partial VTEC}{\partial\phi}$ and $\frac{\partial VTEC}{\partial\lambda}$, and 0.25 (TECU/rad)² for $\frac{\partial^2 VTEC}{\partial\phi^2}$, $\frac{\partial^2 VTEC}{\partial\phi\partial\lambda}$ and $\frac{\partial^2 VTEC}{\partial\lambda^2}$. The model also uses a different mapping function and its dynamics model assumes all reference states are zero. The difference in mapping function prevents a perfect comparison to the model of Reference [1]. These results are presented in Table 3.

Table 3 RMS TEC errors for a given set of data, for 4 different thin-shell models

	RMS TEC errors (removed lines of sight)
Model 1	6.4 (TECU)
Model 2	6.7 (TECU)
Model 3	5.5 (TECU)
Skone Model (Ref. [1])	7.2 (TECU)

5 SUMMARY AND CONCLUSIONS

A method has been developed for the removal of ionospheric effects from single frequency non-GPS radio navigation data through the use of data collected from a single collocated dual-frequency GPS receiver. Two new local ionosphere models have been considered, a thick-shell ionosphere model and a thin-shell ionosphere model. These models' states characterize important ionospheric properties by including their nominal values above the receiver and various of their partial derivatives with respect to latitude and longitude. These states enable the model to form Taylor Series approximations in latitude and longitude of such quantities as ionospheric height, VTEC, and, in the case of the thick-shell model, thickness.

Truth model simulation showed that the thick-shell model contains a subset of very weakly observable states. In contrast, the thin-shell model's Taylor Series coefficient states are largely observable. The dynamics models for those Taylor series coefficients are first-order Markov models of variations about nominal values. Tuning of the Markov parameters has been based on International Reference Ionosphere (IRI) dynamic variations, and on experience with real data.

The most successful implementations of the filter use the thin-shell model with either a fixed known height, an unknown constant height that must be estimated, or an unknown height and unknown first partial derivatives of height with respect to latitude and longitude, all of which must be estimated. This third model allows the ionosphere to be tilted.

These models have an ability to fit the IRI model, to fit actual GPS observables, and to predict TEC along unobserved lines of sight. RMS fit errors from the IRI model ranged between 0.1 and 1 TECU, which indicates an acceptable level of model mismatch between their simple Taylor Series and a realistic 3-D electron distribution. RMS prediction errors in the range of 5.5-7 TECU have been demonstrated based on experience with a limited set of actual GPS data.

6 ACKNOWLEDGEMENTS

This work has been supported in part by Boeing Integrated Defense Systems through Contract No. 8CC0789. Peter Yfy is the contract monitor.

The dual-frequency GPS data used in this paper came from the Arecibo SAS group; their assistance is appreciated.

Certain calculations used the Cornell University Center for Advanced Computing's cluster of parallel processors; their assistance is also appreciated.

REFERENCES

- [1] Skone, S., *TECMODEL Operating Manual*, Calgary, Alberta, Canada, 1st ed., October 2006, University of Calgary.
- [2] Coster, A., Gaposchkin, E., and Thornton, L., "Real-Time Ionosphere Monitoring System Using The GPS", Technical Report no. 954, August 1992, Massachusetts Institute of Technology, Lincoln Laboratory.
- [3] Hernandez-Pajares, M., Juan, J., Sanz, J., Orus, R., Garcia-Rigo, A., Feltens, J., Komjathy, A., Schaer, S., and Krankowski, A., "The IGS VTEC maps: a reliable source of ionospheric information since 1998", *Journal of Geodesy*, vol. 83, no. 3-4, pp. 263-275, 2009, DOI:10.1007/s00190-008-0266-1.
- [4] Arikan, F., Nayir, H., Sezen, F., and Arikan, O., "Estimation of single station interfrequency receiver bias using GPS-TEC", *Radio Science*, vol. 43, 2008, RS4004, doi:10.1029/2007RS003785.
- [5] Komjathy, A. and Langley, R., "An Assessment of Predicted and Measured Ionospheric Total Electron Content Using a Regional GPS Network", In *Proceedings of the Institute of Navigation, National Technical Meeting*, Santa Monica, CA, January 1996, University of New Brunswick.
- [6] Misra, P. and Enge, P., *Global Positioning System, Signals, Measurements, and Performance*, Ganga-Jamuna Press, Massachusetts, 2006, pp. 164-169.
- [7] Coco, D., "Variability of GPS Satellite Differential Group Delay", *IEEE Transactions on Aerospace and Electronic Systems*, vol. 27, no. 6, pp. 931-938, November 1991, University of Texas at Austin.
- [8] Feltens, J., "Chapman Profile Approach for 3-D Global TEC Representation", In *Proceedings of the IGS AC Workshop*, 1998, European Space Operations Centre.
- [9] Marini, J., "Correction of satellite tracking data for an arbitrary tropospheric profile", *Radio Science*, vol. 7, no. 2, pp. 223-231, February 1972, Goddard Space Flight Center.
- [10] Bilitza, D., "International Reference Ionosphere 2000", *Radio Science*, vol. 36, no. 2, pp. 261-275, March/April 2001.
- [11] Bar-Shalom, Y., Rong Li, X., and Kirubarajan, T., *Estimation with Applications to Tracking and Navigation*, John Wiley and Sons, New York, 2001, pp. 371-395.
- [12] Bierman, J., *Factorization Methods for Discrete Sequential Estimation*, Academic Press, New York, 1977, pp. 68-112.